Computers and Geotechnics 38 (2011) 504–514

Contents lists available at ScienceDirect

Computers and Geotechnics

journal homepage: www.elsevier.com/locate/compgeo

Stability of a circular tunnel in cohesive-frictional soil subjected to surcharge loading

Kentaro Yamamoto [a,*], Andrei V. Lyamin [b], Daniel W. Wilson [b], Scott W. Sloan [b], Andrew J. Abbo [b]

[a] Department of Ocean Civil Engineering, Kagoshima University, Kagoshima 890-0065, Japan
[b] Centre for Geotechnical and Materials Modelling, University of Newcastle, NSW 2308, Australia

ARTICLE INFO

Article history:
Received 14 December 2010
Received in revised form 22 February 2011
Accepted 23 February 2011
Available online 21 March 2011

Keywords:
Shallow tunnel
Stability
Rigid-block mechanism
Limit analysis
Finite elements

ABSTRACT

The stability of circular tunnels in cohesive-frictional soils subjected to surcharge loading has been investigated theoretically and numerically assuming plane strain conditions. Despite the importance of this problem, previous research on the subject is very limited. At present, no generally accepted design or analysis method is available to evaluate the stability of tunnels/openings in cohesive-frictional soils. In this study, continuous loading is applied to the ground surface, and both smooth and rough interface conditions are modelled. For a series of tunnel diameter-to-depth ratios and material properties, rigorous lower- and upper-bound solutions for the ultimate surcharge loading are obtained by applying finite element limit analysis techniques. For practical use, the results are presented in the form of dimensionless stability charts with the actual tunnel stability numbers being closely bracketed from above and below. As an additional check on the solutions, upper-bound rigid-block mechanisms have been developed and the predicted collapse loads from these are compared with those from finite element limit analysis. Finally, an expression that approximates the ultimate surcharge load has been devised which is convenient for use by practising engineers.

1. Introduction

Accurately assessing the stability of circular tunnels, pipelines and disused mine workings in cohesive-frictional soils is an important task due to the ubiquitous construction of buildings and tunnels in urban areas. Since many tunnels and pipelines already exist at deep levels, new tunnels and openings are now often being constructed at shallow depths. In these cases, it is important to know how the stability of these tunnels/openings is affected by surcharge loading. As no generally accepted design or analysis method is available currently for this problem, the goal of this study is to equip design engineers with simple design tools to determine the stability of circular tunnels in cohesive-frictional soils subjected to surcharge loading. Drained loading conditions are considered, and a continuous load is applied to the ground surface with both smooth and rough interface conditions. For a series of tunnel diameter-to-depth ratios and material properties, rigorous lower- and upper-bound solutions for the ultimate surcharge loading are found by applying finite element limit analysis techniques [1,2]. The results are presented as dimensionless stability charts for use by practising engineers, and the actual tunnel stability numbers closely bracketed from above and below. As an additional check on the accuracy of the results, a variety of upper-bound rigid-block mechanisms are developed and the solutions from these are compared with those from finite element limit analysis.

The stability of circular tunnels was studied extensively studied at Cambridge in the 1970s; see, for example, the work reported by Cairncross [3], Atkinson and Cairncross [4], Mair [5],

Seneviratne [6] and Davis et al. [7]. Later, theoretical solutions for circular tunnel problems under drained conditions were determined by Muhlhaus [8] and Leca and Dormieux [9].

The application of finite element limit analysis to the undrained stability of shallow tunnels was first considered by Sloan and Assadi [10], who investigated the case of a plane strain circular tunnel in cohesive soil whose shear strength varied linearly with depth using linear programming techniques. Later, Lyamin and Sloan [11] considered the stability of a plane strain circular tunnel in a cohesive-frictional soil using a more efficient non-linear programming technique. This method can accommodate large numbers of finite elements, thus resulting in very accurate solutions. Recently, Yamamoto et al. [12] studied the stability of shallow circular and square tunnels in cohesive-frictional soils subjected to surcharge loading, which is developed further in the present paper.

2. Problem description

The problem description is given in Fig. 1. The ground is modelled as a uniform Mohr–Coulomb material with a cohesion c', friction angle ϕ' and unit weight γ, assuming drained loading

* Corresponding author. Tel.: +81 99 285 8475.
E-mail address: yamaken@oce.kagoshima-u.ac.jp (K. Yamamoto).

0266-352X/$ - see front matter © 2011 Elsevier Ltd. All rights reserved.
doi:10.1016/j.compgeo.2011.02.014

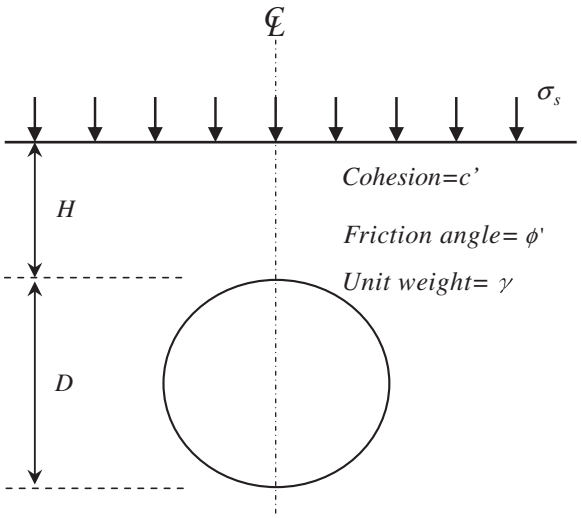

Fig. 1. Plane strain circular tunnel in cohesive-frictional soil.

conditions. The circular tunnel is of diameter D and depth H, and deformation takes place under plane strain. The stability of the shallow tunnel shown in Fig. 1 is described conveniently by the dimensionless load parameter σ_s/c', which is a function of ϕ', $\gamma D/c'$ and H/D as shown in the following equation:

$$\sigma_s/c' = f(\phi', \gamma D/c', H/D) \tag{1}$$

Formulating the problem in this manner permits a compact set of stability charts to be constructed, which are useful for design purposes. The problem parameters considered in this paper are $H/D = 1$–5, $\phi' = 0$–35° and $\gamma D/c' = 0$–3. The continuous (flexible) loading is applied to the ground surface with both smooth and rough interface conditions. To model the smooth interface condition between the loading and the soil, the shear stress is fixed to zero ($\tau = 0$) along the ground surface in the lower-bound analyses, with no velocity constraints being imposed in the upper-bound analyses. For the rough case, the horizontal velocity is fixed to zero ($u = 0$) along the ground surface in the upper-bound analyses, with no stress constraints being imposed in the lower-bound analyses.

3. Finite element limit analysis

Finite element limit analysis utilises the power of the lower- and upper-bound theorems of plasticity theory, coupled with finite elements, to provide rigorous bounds on collapse loads from both below and above. The underlying limit theorems assume a rigid-plastic soil with an associated flow rule. The use of a finite element discretization of the soil, combined with mathematical optimisation to maximise the lower bound and minimise the upper bound, makes it possible to handle problems with layered soils, complex geometries and complicated loading conditions. The formulations of the numerical limit analysis used in this paper originate from those given by Sloan [13,14] and Sloan and Kleeman [15], who employed active-set linear programming and discontinuous stress and velocity fields to solve a variety of practical stability problems. Since then, numerical limit analysis has evolved significantly with the advent of very fast non-linear optimisation solvers, and the techniques used in this paper are those described by Lyamin and Sloan [1] and Krabbenhøft et al. [2].

Briefly, these formulations use linear stress (lower bound) and linear velocity (upper bound) triangular finite elements to discretize the soil mass. In contrast to conventional displacement finite element analysis, each node in the limit analysis mesh is unique to a particular element so that statically admissible stress and kinematically admissible velocity discontinuities are permitted in, respectively, the lower-bound and upper-bound formulations. The objective of the lower-bound analysis is to maximise the load multiplier subject to the element equilibrium, stress boundary conditions and yield constraints. For the upper-bound analysis, the internal power dissipation minus the rate of work done by the prescribed external forces is minimised with respect to the velocity boundary conditions, compatibility and flow rule constraints. Both formulations result in convex mathematical programs, which (after considering the dual to the upper-bound optimisation problem) can be cast in the following form:

$$\begin{aligned} &\text{Maximise} \quad \lambda \\ &\text{subject to } \mathbf{A}\boldsymbol{\sigma} = \mathbf{p}_0 + \lambda \mathbf{p} \\ &f_i(\boldsymbol{\sigma}) \leqslant 0, \quad i = \{1, \ldots, N\} \end{aligned} \tag{2}$$

where λ is a load multiplier, $\boldsymbol{\sigma}$ is a vector of stress variables, $\mathbf{A}$ is a matrix of equality constraint coefficients, $\mathbf{p}_0$ and $\mathbf{p}$ are vectors of prescribed and optimizable forces, f_i is the yield function for the stress set i, and N is the number of stress nodes.

The solutions to problem (2) can be found very efficiently by solving the system of non-linear equations that define its Kuhn-Tucker optimality conditions. The interior point procedure used is based on efficient conic programming implementation, requires usually 30–50 iterations, regardless of the problem size, and is many times faster than previously employed linear programming schemes. The solutions of the lower- and upper-bound computations bracket the actual collapse load from below and above and, thus, give a clear indication of the accuracy of the results.

Fig. 2a and b shows the lower-bound and upper-bound half-meshes for $H/D = 3$ with rough interfaces. The meshes are symmetric, and similar meshes are used for the lower- and upper-bound analyses. The lower-bound mesh has 20,000 triangular elements and 29,850 stress discontinuities, while the upper-bound mesh has 28,800 triangular elements and 43,020 velocity discontinuities. In the lower-bound analysis, extension elements are included along the soil domain boundaries to represent a semi-infinite material. This feature is necessary to guarantee that the lower bounds are fully rigorous, and is a convenient means of extending the stress field throughout a semi-infinite domain in a manner which satisfies equilibrium, the stress boundary conditions and the yield criterion. The size of the soil domain for each of the tunnel geometries considered is chosen such that the plasticity zone at failure lies well inside the domain. Careful mesh refinement is required to obtain accurate solutions, with the mesh density being high around the tunnel face with a smooth transition to larger elements near the boundary of the mesh.

4. Upper-bound rigid-block analysis

Semi-analytical rigid-block methods were used to find upper-bound solutions for the cases considered. These provided an additional check on the limit analysis results. Six types of rigid-block mechanisms were constructed, as shown in Fig. 3. In this Figure, A_i is the area of the rigid block i; V_i is the kinematically admissible velocity of block i; V_{ij} is the velocity jump along the discontinuity between blocks i and j; l_{ij} is the distance between points i and j; (α, β, γ, δ, ε, λ, ω) are angles that determine the geometry of the rigid-block mechanism; and ϕ' is the dilatancy angle. The compatible velocity diagrams using V_i and V_{ij} are given at the right side of the block mechanisms. All velocities can be obtained using the geometry of these diagrams. With an associated flow rule we

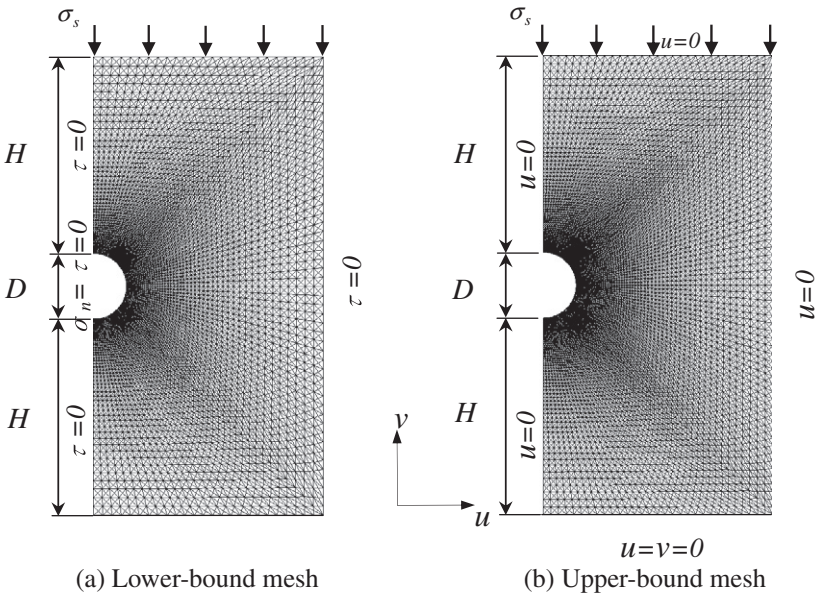

(a) Lower-bound mesh (b) Upper-bound mesh

Fig. 2. Typical finite element meshes for a circular tunnel ($H/D = 3$, rough interface).

assume the dilatancy angle is equal to the friction angle. Although it is well known that the use of an associated flow rule predicts excessive dilation during shear failure of frictional soils, it is unlikely this feature will have a major impact on the predicted limit loads for cases with low to moderate friction angles. Generally speaking, any inaccuracy caused by an associated flow rule will be most pronounced for soils with very high friction angles and/or problems that are subject to high degrees of kinematic constraint (which is not the case for the tunnel considered here). Mechanism 1 is a simple roof collapse mechanism which is suitable for shallow tunnels, while the mechanisms 2–6 are more complex examples of both roof and side collapse mechanisms. The total number of angular parameters for mechanisms 1–6 are 1, 4, 7, 4, 3 and 7, respectively. The soil mass was assumed to be governed by the Mohr–Coulomb failure criterion and an associated flow rule, with the geometry of the blocks being allowed to vary while being constrained such that their areas and boundary segment lengths remain non-negative. The details of rigid-block analysis can be found in Chen [16]. The upper-bound solutions derived from mechanisms 1–6 are given as follows:

Mechanism 1

$$\sigma_s \leqslant \frac{c' l_{cd} \cos\phi' - A_1\gamma}{l_{ad}} \tag{3}$$

Mechanism 2

$$\sigma_s \leqslant \frac{c('V_1 l_{ef} \cos\phi' + V_2 l_{de} \cos\phi' + V_{21} l_{ce} \cos\phi') - \gamma(A_1V_1 + A_2V_2 \sin(\gamma - \phi'))}{V_1 l_{af}} \tag{4}$$

Mechanism 3

$$\sigma_s \leqslant \frac{c'(V_1 l_{gh} \cos\phi' + V_2 l_{fg} \cos\phi' + V_{21} l_{cg} \cos\phi' + V_3 l_{ef} \cos\phi' + V_{32} l_{df} \cos\phi') - \gamma(A_1V_1 + A_2V_2 \sin(\varepsilon - \phi') + A_3V_3 \sin(\delta - \phi'))}{V_1 l_{ah}} \tag{5}$$

Mechanism 4

$$\sigma_s \leqslant \frac{c'(V_2 l_{de} \cos\phi' + V_{21} l_{ad} \cos\phi' + V_{31} l_{bd} \cos\phi' + V_3 l_{cd} \cos\phi') - \gamma(A_1V_1 + A_2V_2 \sin(\delta - \phi') + A_3V_3 \sin(\gamma - \phi'))}{V_2 l_{ae} \sin(\delta - \phi')} \tag{6}$$

Mechanism 5

$$\sigma_s \leqslant \frac{c'(V_2 l_{de} \cos\phi' + V_{21} l_{be} \cos\phi' + V_{32} l_{bd} \cos\phi' + V_3 l_{cd} \cos\phi') - \gamma(A_1V_1 + A_2V_2 \sin(\delta - \phi') + A_3V_3 \sin(\beta - \phi'))}{V_1 l_{ae}} \tag{7}$$

Mechanism 6

$$\sigma_s \leqslant \frac{c'(V_2 l_{fg} \cos\phi' + V_{21} l_{af} \cos\phi' + V_{31} l_{bf} \cos\phi' + V_3 l_{ef} \cos\phi' + V_{43} l_{ce} \cos\phi\prime + V_4 l_{de} \cos\phi')}{V_2 l_{ag} \sin(\delta - \phi')} \times \frac{-\gamma(A_1V_1 + A_2V_2 \sin(\delta - \phi') + A_3V_3 \sin(\omega - \phi') + A_4V_4 \sin(\lambda - \phi'))}{V_2 l_{ag} \sin(\delta - \phi')} \tag{8}$$

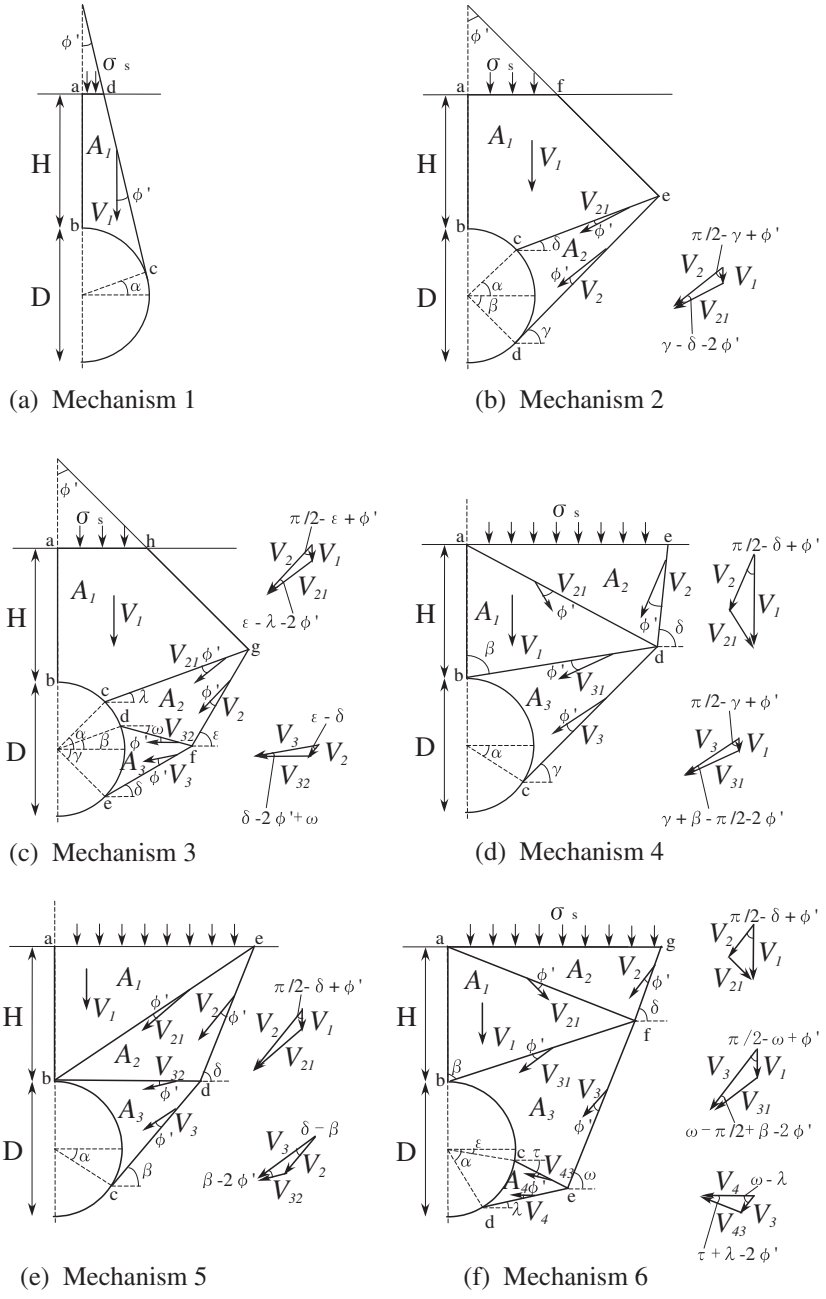

Fig. 3. Upper-bound rigid-block mechanisms for a circular tunnel.

The minimum upper-bound solution for each mechanism was obtained by optimising its geometry using the Hooke and Jeeves' algorithm with discrete steps (Bunday [17]). This method works by performing two different types of searches: an exploratory search and a pattern search. The rigid-block analyses are fast and, provided an appropriate mechanism is chosen, can give useful upper-bounds on the true collapse load. These solutions can also be used to check the finite element limit analysis solutions.

Table 1 shows the comparison of the upper-bound solutions obtained from mechanisms 1–6 for $H/D = 1$–3, $\phi' = 0$–20° and $\gamma D/c' = 0$–3. It is found that the upper-bound solutions from the different mechanisms increase in the following order: Mechanism 3, Mechanism 6, Mechanism 2, Mechanism 4, Mechanism 5 and Mechanism 1. Note that the solutions from Mechanism 6 are larger than those from Mechanism 2 for $H/D = 1$, $\phi' \geqslant 5°$ and $\gamma D/c' = 0$–3, and the solutions from Mechanism 1 tend to be infeasible due to geometry constraints for the cases of high ϕ' when H/D increases. As expected, the best upper-bound solution is given by Mechanism 3, which has the largest number of variables with three rigid blocks and seven angular parameters.

5. Results and discussion

Figs. 4–7a–d show the rigid-block mechanisms, power dissipations, deformed meshes and plastic multiplier field for the various cases. The optimum rigid-block mechanism is obtained from the upper-bound rigid-block analysis, and the power dissipation, deformed mesh and the plastic multiplier field are obtained from the finite element upper-bound and lower-bound analyses. The intensity of the power dissipation and the plastic multiplier field

Table 1
Comparison of the upper-bound solutions from various rigid-block mechanisms.

H/D	ϕ' (°)	Mechanism 1				Mechanism 2				Mechanism 3			
		$\gamma D/c'=0$	$\gamma D/c'=1$	$\gamma D/c'=2$	$\gamma D/c'=3$	$\gamma D/c'=0$	$\gamma D/c'=1$	$\gamma D/c'=2$	$\gamma D/c'=3$	$\gamma D/c'=0$	$\gamma D/c'=1$	$\gamma D/c'=2$	$\gamma D/c'=3$
1	0	2.83	1.74	0.64	−0.45	2.56	1.40	0.22	−1.00	2.54	1.36	0.13	−1.15
	5	3.76	2.53	1.30	0.07	3.15	1.89	0.62	−0.67	3.10	1.81	0.50	−0.84
	10	5.64	4.13	2.62	1.11	4.04	2.64	1.23	−0.19	3.92	2.49	1.04	−0.43
	15	11.68	9.26	6.84	4.42	5.52	3.89	2.25	0.60	5.23	3.58	1.91	0.23
	20	–	–	–	–	8.39	6.36	4.31	2.24	7.57	5.55	3.52	1.46
2	0	4.90	2.80	0.70	−1.41	3.78	1.56	−0.70	−2.99	3.68	1.40	−0.93	−3.29
	5	8.57	5.80	0.24	0.24	5.10	2.59	0.07	−2.47	4.85	2.30	−0.27	−2.85
	10	35.98	28.16	6.18	12.50	7.53	4.54	1.52	−1.55	6.87	3.89	0.87	−2.18
	15	–	–	–	–	13.14	9.20	5.16	0.93	10.99	7.23	3.37	−0.64
	20	–	–	–	–	33.61	26.95	20.06	12.78	22.07	16.65	11.00	4.92
3	0	6.93	3.82	0.72	−2.38	4.71	1.45	−1.85	−5.17	4.50	1.17	−2.21	−5.62
	5	17.59	12.35	7.10	1.85	6.85	3.06	−0.75	−4.60	6.31	2.50	−1.33	−5.18
	10	–	–	–	–	11.58	6.77	1.83	−3.36	9.88	5.23	0.48	−4.49
	15	–	–	–	–	27.35	19.88	12.05	3.36	19.08	12.70	5.96	−1.68
	20	–	–	–	–	229.19	201.39	172.78	142.98	58.97	47.62	35.57	22.22

H/D	ϕ' (°)	Mechanism 4				Mechanism 5				Mechanism 6			
		$\gamma D/c'=0$	$\gamma D/c'=1$	$\gamma D/c'=2$	$\gamma D/c'=3$	$\gamma D/c'=0$	$\gamma D/c'=1$	$\gamma D/c'=2$	$\gamma D/c'=3$	$\gamma D/c'=0$	$\gamma D/c'=1$	$\gamma D/c'=2$	$\gamma D/c'=3$
1	0	2.62	1.49	0.34	−0.82	2.65	1.51	0.35	−0.82	2.55	1.39	0.19	−1.05
	5	3.22	1.99	0.75	−0.50	3.26	2.01	0.77	−0.49	3.22	1.95	0.67	−0.64
	10	4.13	2.75	1.36	−0.02	4.18	2.78	1.39	0.00	4.24	2.80	1.36	−0.09
	15	5.64	4.03	2.41	0.79	5.69	4.08	2.45	0.82	5.89	4.19	2.48	0.77
	20	8.55	6.53	4.50	2.45	8.69	6.71	4.72	2.74	8.95	6.79	4.62	2.42
2	0	3.84	1.65	−0.56	−2.78	3.87	1.67	−0.55	−2.78	3.69	1.43	−0.87	−3.21
	5	5.18	2.70	0.21	−2.28	5.21	2.72	0.22	−2.27	4.98	2.45	−0.09	−2.65
	10	7.63	4.66	1.67	−1.35	7.68	4.71	1.71	−1.32	7.29	4.28	1.24	−1.82
	15	13.28	9.35	5.33	1.15	13.63	9.87	6.11	2.35	12.09	8.19	4.21	0.09
	20	33.86	27.17	20.26	12.98	–	–	–	–	25.41	19.59	13.53	7.04
3	0	4.77	1.54	−1.71	−4.97	4.80	1.55	−1.71	−4.97	4.51	1.20	−2.16	−5.55
	5	6.92	3.16	−0.62	−4.41	6.96	3.18	−0.60	−4.40	6.52	2.69	−1.14	−4.99
	10	11.68	6.88	1.98	−3.13	11.73	6.94	2.03	−3.01	10.50	5.77	0.95	−4.05
	15	27.51	20.03	12.20	3.57	50.39	43.39	36.40	29.40	20.98	14.36	7.38	−0.43
	20	229.73	201.72	172.93	143.03	–	–	–	–	68.25	56.35	43.62	29.51

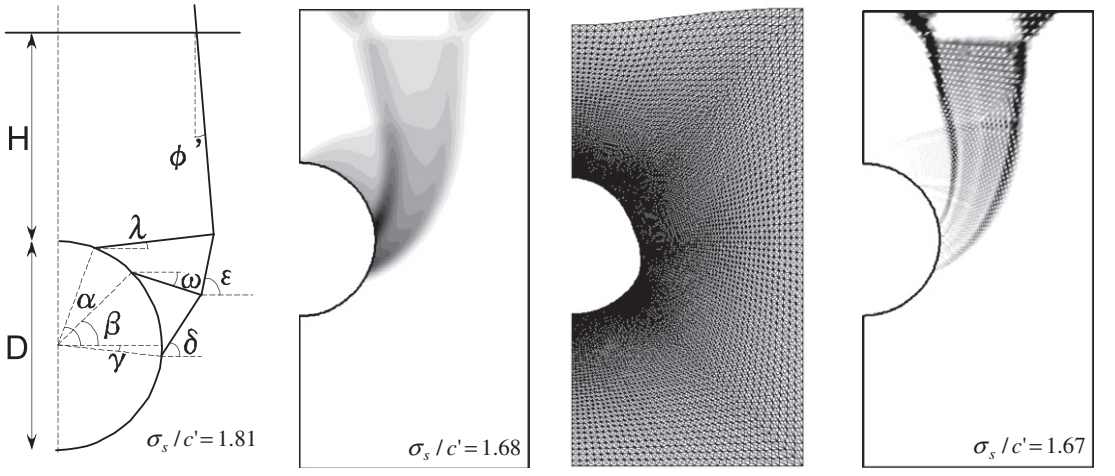

(a) Rigid-block mechanism (b) Power dissipation (c) Deformed mesh (d) Plastic multiplier field

Fig. 4. Comparison of rigid-block mechanism with finite element limit analysis ($H/D = 1$, $\phi' = 5°$, $\gamma D/c' = 1$, smooth interface).

is shown by the grey shading. Lower- and upper-bound estimates of the dimensionless load parameter, σ_s/c', obtained from finite element limit analysis and rigid-block analysis, are included in each figure. In this paper, Eq. (9) is used to measure the gap between the bounds, and is thus a direct estimate of the error in the solutions.

$$Error\ (\%) = \pm 100 \times (UB - LB)/(UB + LB) \tag{9}$$

Generally, the distributions of the power dissipation from the upper-bound analyses agree fairly well with the plastic multiplier field obtained from the lower-bound analyses. Fig. 4b and d shows that, for small friction angles, the failure surface originates around

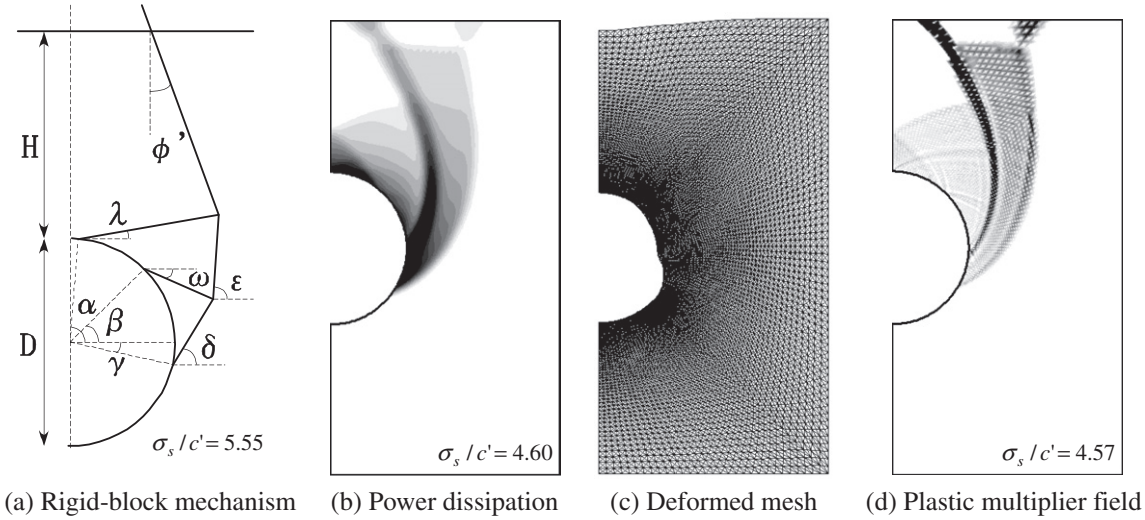

Fig. 5. Comparison of rigid-block mechanism with finite element limit analysis ($H/D = 1$, $\phi' = 20°$, $\gamma D/c' = 1$, smooth interface).

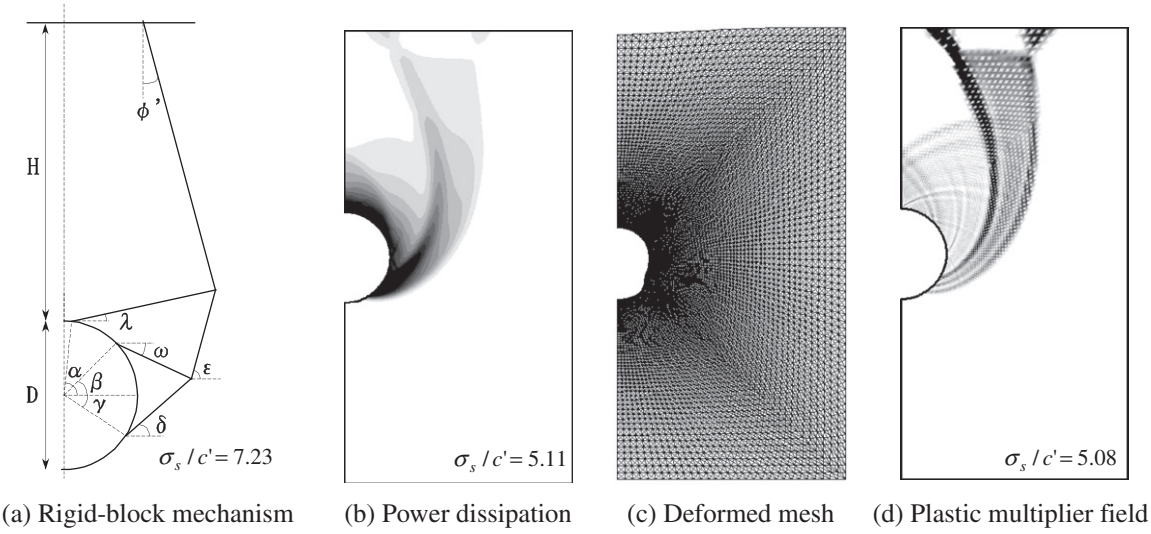

Fig. 6. Comparison of rigid-block mechanism with finite element limit analysis ($H/D = 2$, $\phi' = 15°$, $\gamma D/c' = 1$, smooth interface).

the middle part of the tunnel and curves toward the ground surface. It can also be seen that the failure mechanisms from the rigid-block technique agree well with those observed from finite element limit analysis. For the case of moderate friction angles presented in Fig. 5b and d, the failure surface also originates around the middle part of the tunnel, but its curvature is much more pronounced right above the tunnel. As expected, the ultimate surcharge load in this case is higher than that shown in Fig. 4. For shallow tunnels ($H/D = 1$) shown in Figs. 4 and 5, the failure mechanism is confined to the upper half of the tunnel. When H/D increases, as shown in Figs. 6 and 7, the failure mechanism extends downwards to eventually encompass the entire tunnel. These deeper collapse mechanisms are more complex than those for shallow tunnels. The errors for the cases shown in Figs. 4–7 are 0.3%, 0.3%, 0.4% and 0.8%, respectively. Thus, the rigorous lower- and upper-bound solutions bracket the true ultimate surcharge load quite accurately for soils with moderate frictional angles. In general, the upper-bound solutions obtained from both the rigid-block and finite element limit analyses are in good agreement for smaller values of H/D or ϕ'. For other cases, the accuracy of the first three mechanisms is limited by the assumption that the failure mechanism extends downwards from the ground surface at an angle of ϕ' to the vertical. Deep tunnels develop quite complex collapse patterns, and the simple rigid-block mechanisms proposed in this study are most accurate for shallow cases. Furthermore, due to the effect of dilation along the velocity discontinuities, it is more difficult to formulate an appropriate rigid-block mechanism for cohesive-frictional soils than for purely cohesive soils.

Fig. 8 compares the stability numbers obtained from both rigid-block and finite element limit analyses for a smooth interface condition, with rigid-block results being shown for ϕ' values up to 20°. As expected, the stability numbers decrease when $\gamma D/c'$ increases. For small values of ϕ', the rigorous lower- and upper-bound solutions bracket the true ultimate surcharge load very accurately and cannot be distinguished on the scale of the plot. For $\phi' = 30°$, the stability number increases rapidly with increasing values of H/D, but even in this case the maximum error in the limit analysis computations does not exceed ±6%. For the cases of ($\phi' = 5°$, $H/D \leqslant 5$),

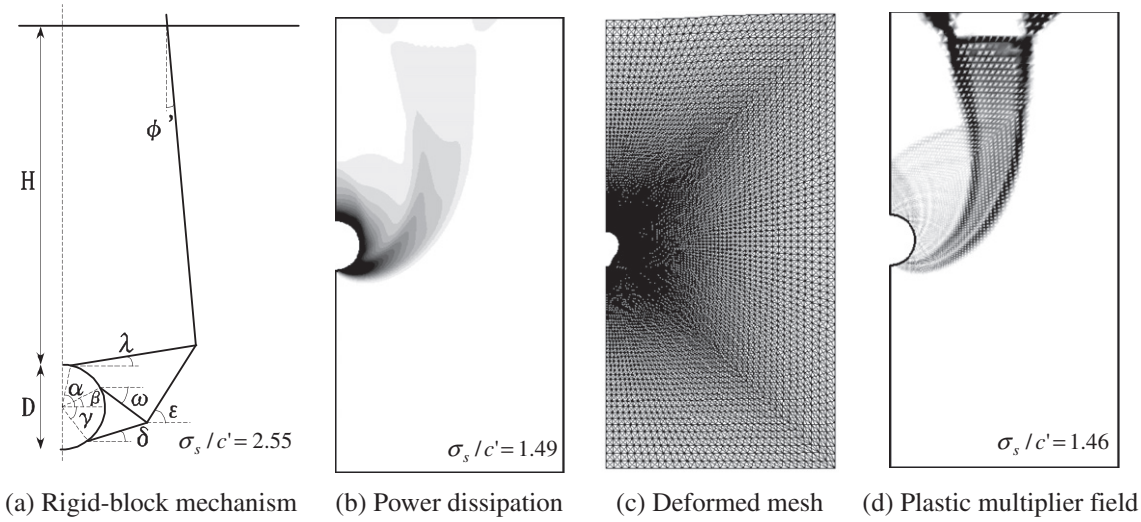

Fig. 7. Comparison of rigid-block mechanism with finite element limit analysis ($H/D = 4$, $\phi' = 5°$, $\gamma D/c' = 1$, smooth interface).

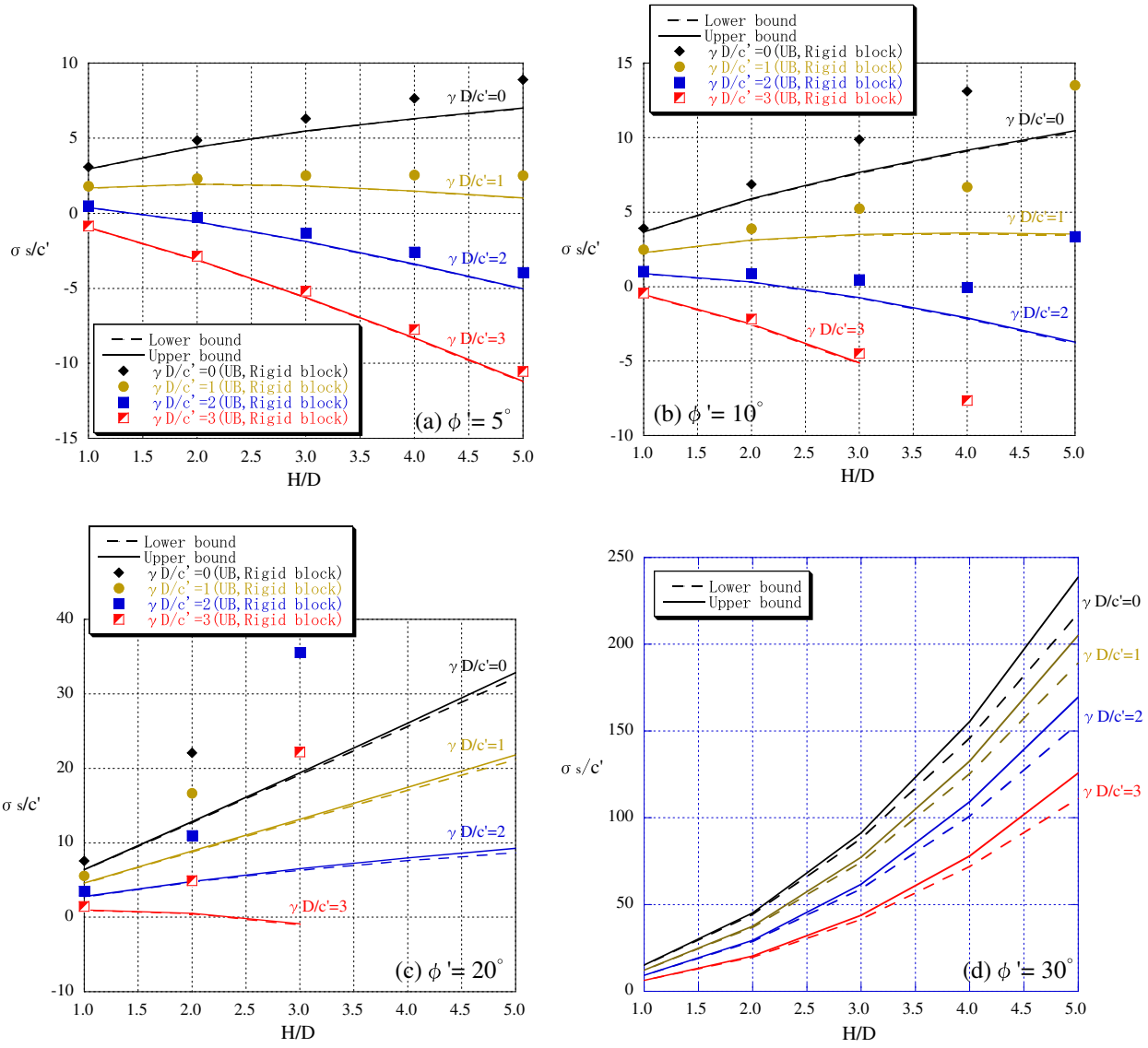

Fig. 8. Stability bounds for a circular tunnel ($\phi' = 5°$, 10°, 20°, 30°, smooth interface).

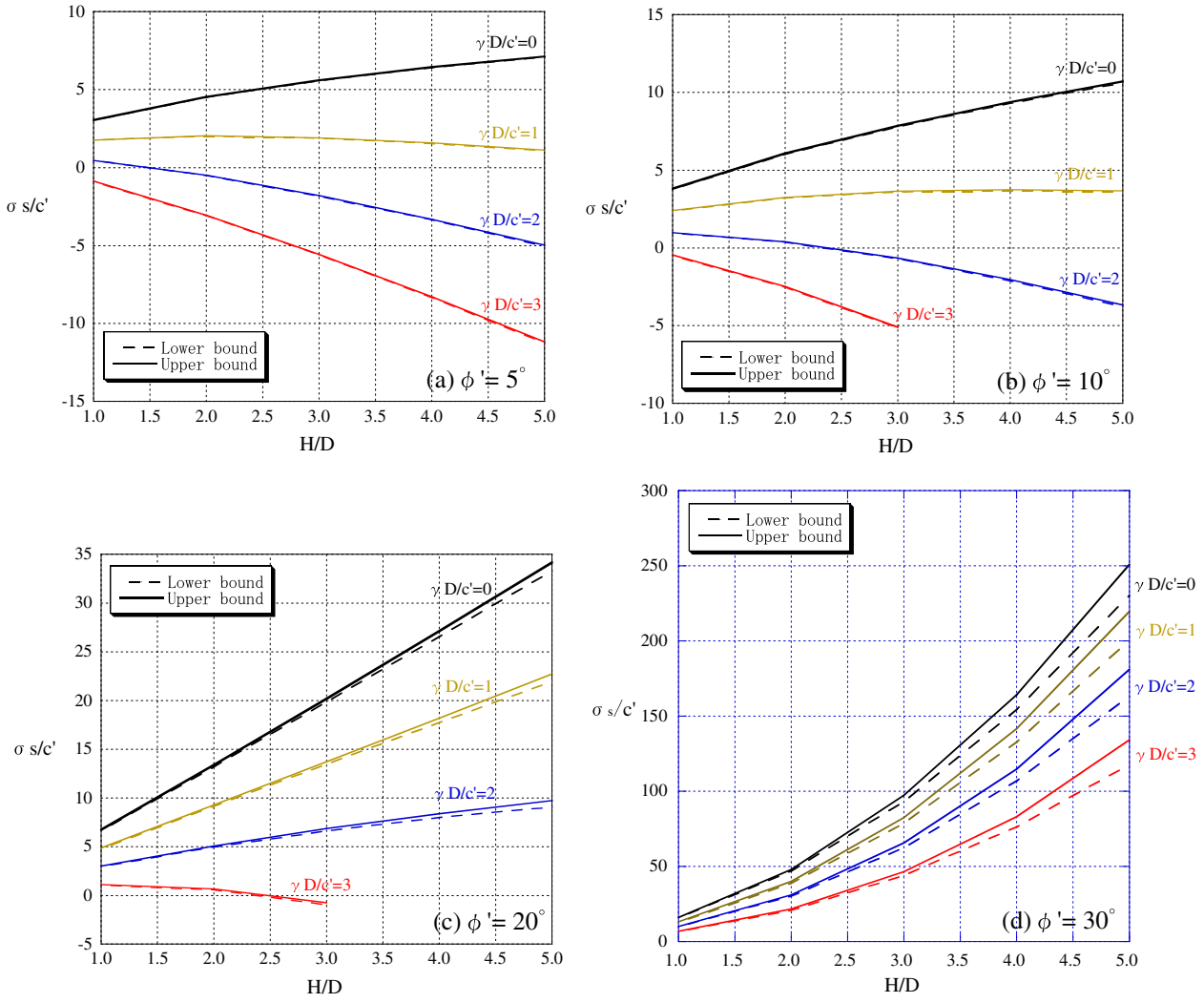

Fig. 9. Stability bounds for a circular tunnel (ϕ' = 5°, 10°, 20°, 30°, rough interface).

Table 2
Coefficients of empirical equation.

Parameters	Smooth interface	Rough interface
a	1.492521	1.558360
b	0.070218	0.068660
c	1.040522	1.059821
d	0.472325	0.466462
e	0.015413	0.016675
f	1.317933	1.295656
g	−0.495490	−0.479079
h	0.010923	0.010225
k	0.464155	0.478401
m	−0.012827	−0.013290

(ϕ' = 10°, $H/D \leqslant 3$) and (ϕ' = 20°, $H/D \leqslant 1$), the upper-bound solutions from the rigid-block method agree well with those obtained from finite element limit analysis. However, for cases with high values of H/D or ϕ', the accuracy of the solutions from all the rigid-block mechanisms becomes poor. In some cases where $\gamma D/c' = 3$ and $H/D \geqslant 4$, as shown in Fig. 8b and c, feasible solutions from the rigid-block and finite element limit analyses could not be obtained because the tunnel undergoes local roof collapse due to the effect of soil self-weight. Note that the sign convention for the stability charts is that a positive value of the stability number implies that the ground can support a compressive normal stress, while a negative stability number means that we can only apply a tensile normal stress to the soil surface. Fig. 9 shows the stability numbers obtained from finite element limit analysis for the case of a rough interface. The general trend of the stability numbers is mostly the same as for the smooth case, but the ultimate surcharge loads are slightly higher with maximum bounds error of ±6%. Therefore, the rigorous lower- and upper-bound solutions bracket the true ultimate surcharge load quite accurately, even in the case of deeper tunnels ($H/D = 5$) and moderate soil friction angles ($\phi' = 30°$).

Finally, based on the results obtained using finite element limit analysis, an expression that approximates the ultimate surcharge loading is as follows:

$$\sigma_s/c' = [a + \exp(b\phi'^c)](H/D)^{d\exp(e\phi'^f)}[1 + (g + h\phi')(H/D)^{k+m\phi'}(\gamma D/c')] \quad (10)$$

where the regression coefficients a, b, c, d, e, f, g, h, k and m are obtained by a least squares fit to the average values of the lower- and upper-bound solutions. Table 2 provides the values of the regression constants for both smooth and rough interface conditions, while Tables 3 and 4 compare the average values from finite element limit analysis with those obtained from Eq. (10). As can be seen from these tables, the stability number σ_s/c' calculated using this empirical equation predicts the average value of the numerical

Table 3
Comparison of the average values from the numerical limit analysis with those obtained from the empirical equation (smooth interface).

ϕ' (°)	H/D	$(LB + UB)/2$				Empirical equation			
		$\gamma D/c' = 0$	$\gamma D/c' = 1$	$\gamma D/c' = 2$	$\gamma D/c' = 3$	$\gamma D/c' = 0$	$\gamma D/c' = 1$	$\gamma D/c' = 2$	$\gamma D/c' = 3$
0	1	2.44	1.26	0.02	−1.28	2.49	1.26	0.02	−1.21
	2	3.46	1.18	−1.16	−3.59	3.46	1.09	−1.27	−3.63
	3	4.13	0.80	−2.60	−6.08	4.19	0.73	−2.72	−6.18
	4	4.64	0.27	−4.17	-8.68	4.80	0.27	−4.25	−8.77
	5	5.04	−0.35	−5.81	−11.34	5.33	−0.24	−5.82	−11.39
5	1	2.94	1.68	0.38	−0.95	2.95	1.65	0.35	−0.95
	2	4.42	1.94	−0.57	−3.12	4.28	1.79	−0.70	−3.19
	3	5.47	1.81	−1.88	−5.62	5.32	1.68	−1.96	−5.60
	4	6.30	1.48	−3.39	−8.33	6.21	1.44	−3.32	−8.09
	5	6.99	1.01	−5.04	−11.21	7.00	1.12	−4.75	−10.62
10	1	3.66	2.27	0.87	−0.55	3.65	2.24	0.83	−0.58
	2	5.89	3.11	0.30	−2.55	5.74	2.94	0.14	−2.65
	3	7.64	3.48	−0.76	−5.13	7.47	3.30	−0.88	−5.05
	4	9.12	3.58	−2.13	–	9.01	3.46	−2.08	−7.62
	5	10.42	3.49	−3.76	–	10.41	3.51	−3.40	−10.31
15	1	4.70	3.15	1.60	0.02	4.73	3.16	1.59	0.02
	2	8.32	5.09	1.81	−1.57	8.33	5.00	1.66	−1.68
	3	11.51	6.58	1.44	–	11.60	6.41	1.23	−3.96
	4	14.44	7.77	0.66	–	14.67	7.58	0.49	−6.60
	5	17.18	8.74	−0.48	–	17.60	8.56	−0.48	−9.52
20	1	6.38	4.59	2.79	0.96	6.37	4.61	2.84	1.08
	2	12.77	8.84	4.78	0.49	13.20	8.98	4.75	0.53
	3	19.26	13.06	6.42	−0.96	20.21	13.18	6.14	−0.89
	4	25.84	17.27	7.80	–	27.34	17.24	7.14	−2.96
	5	32.50	21.48	8.95	–	34.55	21.18	7.81	−5.56
25	1	9.28	7.11	4.91	2.68	8.88	6.91	4.93	2.96
	2	22.01	16.86	11.41	5.58	23.12	17.44	11.76	6.08
	3	37.45	28.89	19.47	8.85	40.45	29.92	19.39	8.85
	4	55.15	42.92	28.91	12.47	60.17	43.84	27.52	11.19
	5	74.93	58.79	39.71	16.52	81.87	58.93	35.99	13.05
30	1	14.98	12.15	9.27	6.30	12.71	10.58	8.45	6.31
	2	44.73	37.14	28.96	20.05	45.73	37.62	29.51	21.41
	3	89.58	75.91	60.37	42.59	96.68	78.98	61.28	43.58
	4	150.65	129.01	105.14	75.00	164.46	133.66	102.85	72.05
	5	228.03	197.16	161.85	118.46	248.33	200.99	153.64	106.30
35	1	28.04	23.91	19.66	15.26	18.58	16.48	14.38	12.27
	2	115.57	101.99	86.99	70.42	105.89	93.78	81.67	69.56
	3	289.34	261.33	228.42	190.11	293.05	259.33	225.60	191.88
	4	581.10	533.68	474.96	398.03	603.41	533.66	463.92	394.17
	5	1013.81	942.38	853.55	739.79	1056.60	934.06	811.51	688.96

Table 4
Comparison of the average values from the numerical limit analysis with those obtained from the empirical equation (rough interface).

ϕ' (°)	H/D	$(LB + UB)/2$				Empirical equation			
		$\gamma D/c' = 0$	$\gamma D/c' = 1$	$\gamma D/c' = 2$	$\gamma D/c' = 3$	$\gamma D/c' = 0$	$\gamma D/c' = 1$	$\gamma D/c' = 2$	$\gamma D/c' = 3$
0	1	2.51	1.33	0.10	−1.22	2.56	1.33	0.11	−1.12
	2	3.53	1.26	−1.09	−3.53	3.53	1.18	−1.18	−3.54
	3	4.21	0.88	−2.53	−6.01	4.27	0.81	−2.65	−6.11
	4	4.71	0.35	−4.09	−8.61	4.88	0.34	−4.20	−8.74
	5	5.11	−0.28	−5.74	−11.27	5.42	−0.19	−5.80	−11.40
5	1	3.04	1.77	0.46	−0.88	3.02	1.73	0.43	−0.86
	2	4.52	2.03	−0.50	−3.07	4.37	1.88	−0.61	−3.09
	3	5.58	1.90	−1.82	−5.57	5.42	1.77	−1.88	−5.52
	4	6.42	1.56	−3.34	−8.30	6.32	1.53	−3.26	−8.05
	5	7.12	1.10	−4.99	−11.20	7.12	1.21	−4.71	−10.62
10	1	3.79	2.39	0.97	−0.48	3.76	2.34	0.93	−0.49
	2	6.05	3.23	0.39	−2.50	5.89	3.07	0.25	−2.57
	3	7.83	3.62	−0.68	−5.11	7.66	3.44	−0.78	−5.00
	4	9.34	3.72	−2.07	–	9.23	3.62	−2.00	−7.62
	5	10.66	3.63	−3.71	–	10.67	3.66	−3.35	−10.36
15	1	4.90	3.31	1.72	0.11	4.92	3.31	1.71	0.11
	2	8.60	5.30	1.94	−1.51	8.64	5.23	1.81	−1.60
	3	11.87	6.82	1.58	–	12.02	6.70	1.38	−3.94
	4	14.87	8.05	0.78	–	15.20	7.91	0.62	−6.67
	5	17.68	9.05	−0.38	–	18.22	8.92	−0.38	−9.68
20	1	6.69	4.83	2.98	1.09	6.73	4.88	3.03	1.19
	2	13.31	9.23	5.03	0.62	13.90	9.48	5.06	0.63
	3	20.02	13.60	6.75	−0.86	21.25	13.88	6.51	−0.86
	4	26.84	17.97	8.19	–	28.73	18.14	7.54	−3.05
	5	33.74	22.34	9.39	–	36.29	22.26	8.23	−5.80
25	1	9.78	7.52	5.23	2.90	9.57	7.43	5.29	3.16
	2	23.09	17.70	12.03	5.96	24.79	18.66	12.53	6.40
	3	39.27	30.31	20.46	9.39	43.26	31.91	20.56	9.21
	4	57.84	45.02	30.37	13.19	64.22	46.65	29.07	11.50
	5	78.60	61.67	41.69	17.43	87.25	62.58	37.92	13.25
30	1	15.92	12.94	9.90	6.79	14.04	11.62	9.20	6.78
	2	47.43	39.41	30.72	21.28	49.96	40.86	31.77	22.67
	3	95.21	80.67	64.14	45.29	104.97	85.23	65.48	45.74
	4	159.33	137.23	110.96	79.78	177.75	143.54	109.33	75.12
	5	240.57	209.98	172.28	125.96	267.46	215.06	162.66	110.26
35	1	30.06	25.61	21.11	16.41	21.10	18.54	15.99	13.43
	2	123.85	109.31	93.36	75.73	117.49	103.12	88.75	74.38
	3	312.86	282.38	246.78	205.33	320.79	281.34	241.89	202.44
	4	622.25	571.22	508.04	431.13	654.20	573.44	492.68	411.92
	5	1076.84	999.53	903.00	781.57	1137.03	996.25	855.47	714.70

solutions quite accurately, being to within 5% for all the values of H/D and ϕ' considered.

6. Conclusions

The stability of a plane strain circular tunnel, in a cohesive-frictional soil subjected to surcharge loading, has been investigated using upper-bound rigid-block analysis and finite element limit analysis. The results of these analyses have been presented in the form of dimensionless stability charts. The lower and upper-bounds obtained using finite element limit analysis bracket the actual ultimate surcharge load to within ±6% or better. As an additional check of the validity of the finite element limit analysis results, several upper-bound rigid-block mechanisms were developed. A comparison of the upper-bound solutions obtained from the rigid-block analysis with those of finite element limit analysis shows good agreement when ϕ' and H/D are small. An empirical equation for estimating the ultimate surcharge load that can be applied to the surface of a cohesive-frictional soil above a shallow circular tunnel has been proposed. This equation is based on average values of the lower- and upper-bound solutions from finite element limit analysis, and predicts these values to within 5%.

References

[1] Lyamin AV, Sloan SW. Lower bound limit analysis using non-linear programming. Int J Numer Meth Eng 2002;55:573–611.
[2] Krabbenhøft K, Lyamin AV, Hjiaj M, Sloan SW. A new discontinuous upper bound limit analysis formulation. Int J Numer Meth Eng 2005;63:1069–88.
[3] Cairncross AM. Deformation around model tunnels in stiff clay. PhD thesis. University of Cambridge; 1973.
[4] Atkinson JH, Cairncross AM. Collapse of a shallow tunnel in a Mohr-Coulomb material. In: Role of plasticity in soil mechanics, Cambridge; 1973. p. 202–06.
[5] Mair RJ. Centrifugal modelling of tunnel construction in soft clay. PhD thesis. University of Cambridge; 1979.
[6] Seneviratne HN. Deformations and pore-pressures around model tunnels in soft clay. PhD thesis. University of Cambridge; 1979.
[7] Davis EH, Gunn MJ, Mair RJ, Seneviratne HN. The stability of shallow tunnels and underground openings in cohesive material. Geotechnique 1980;30(4): 397–416.
[8] Muhlhaus HB. Lower bound solutions for circular tunnels in two and three dimensions. Rock Mech Rock Eng 1985;18:37–52.
[9] Leca E, Dormieux L. Upper and lower bound solutions for the face stability of shallow circular tunnels in frictional material. Geotechnique 1990;40(4): 581–606.
[10] Sloan SW, Assadi A. Stability of shallow tunnels in soft ground. In: Holsby GT, Schofield AN, editors. Predictive soil mechanics. London: Thomas Telford; 1993. p. 644–63.
[11] Lyamin AV, Sloan SW. Stability of a plane strain circular tunnel in a cohesive-frictional soil. In: Proceedings of the J.R. Booker Memorial symposium, Sydney; 2000. p. 139–53.
[12] Yamamoto K, Lyamin AV, Sloan SW, Abbo AJ. Bearing capacity of a cohesive-frictional soil with a shallow tunnel. In: Proc. 13th Asian regional conf on soil mechanics and geotech eng, vol. 1, Kolkata; 2007. p. 489–92.
[13] Sloan SW. Lower bound limit analysis using finite elements and linear programming. Int J Numer Analyt Meth Geomech 1988;12:61–77.
[14] Sloan SW. Upper bound limit analysis using finite elements and linear programming. Int J Numer Analyt Meth Geomech 1989;13:263–82.
[15] Sloan SW, Kleeman PW. Upper bound limit analysis using discontinuous velocity fields. Comput Methods Appl Mech Eng 1995;127:293–314.
[16] Chen WF. Limit analysis and soil plasticity. Amsterdam: Elsevier; 1975.
[17] Bunday BD. Basic optimisation methods. Edward Arnold; 1984.